



This is a repository copy of *Characterization, simulation and control of a soft helical pneumatic implantable robot for tissue regeneration*.

White Rose Research Online URL for this paper:
<http://eprints.whiterose.ac.uk/156148/>

Version: Accepted Version

Article:

Perez Guagnelli, E.R. orcid.org/0000-0001-5600-1561, Jones, J., Tokel, A.H. et al. (4 more authors) (2020) Characterization, simulation and control of a soft helical pneumatic implantable robot for tissue regeneration. *IEEE Transactions on Medical Robotics and Bionics*, 2 (1). pp. 94-103. ISSN 2576-3202

<https://doi.org/10.1109/TMRB.2020.2970308>

© 2020 IEEE. Personal use of this material is permitted. Permission from IEEE must be obtained for all other users, including reprinting/ republishing this material for advertising or promotional purposes, creating new collective works for resale or redistribution to servers or lists, or reuse of any copyrighted components of this work in other works. Reproduced in accordance with the publisher's self-archiving policy.

Reuse

Items deposited in White Rose Research Online are protected by copyright, with all rights reserved unless indicated otherwise. They may be downloaded and/or printed for private study, or other acts as permitted by national copyright laws. The publisher or other rights holders may allow further reproduction and re-use of the full text version. This is indicated by the licence information on the White Rose Research Online record for the item.

Takedown

If you consider content in White Rose Research Online to be in breach of UK law, please notify us by emailing eprints@whiterose.ac.uk including the URL of the record and the reason for the withdrawal request.



eprints@whiterose.ac.uk
<https://eprints.whiterose.ac.uk/>

Characterization, Simulation and Control of a Soft Helical Pneumatic Implantable Robot for Tissue Regeneration

Eduardo Perez-Guagnelli^{1†}, Joanna Jones^{1†}, Ahmet H. Tokel¹, Nicolas Herzig¹, Bryn Jones¹, Shuhei Miyashita¹ and Dana D. Damian¹

Abstract—Therapies for tissue repair and regeneration have remained sub-optimal, with limited approaches investigated to improve their effectiveness, dynamic and control response. We introduce a Soft Pneumatic Helically-Interlayered Actuator (SoPHIA) for tissue repair and regeneration of tubular tissues. The actuator features shape configurability in two and three dimensions for minimal or non-invasive *in vivo* implantation; multi-modal therapy to apply mechanical stimulation axially and radially, in accordance to the anatomy of tubular tissues; and anti-buckling structural strength. We present a model and characteristics of this soft actuator. SoPHIA reaches up to 36.3% of elongation with respect to its initial height and up to 7N of force when pressurized at 38 kPa against anatomically-realistic spatial constraints. Furthermore, we introduce the capabilities of a physical *in vivo* simulator of biological tissue stiffness and growth, for the evaluation of the soft actuator in physiologically-relevant conditions. Lastly, we propose a model-based multi-stage control of the axial elongation of the actuator according to the tissue’s physiological response. SoPHIA has the potential to reduce the invasiveness of surgical interventions and increase the effectiveness in growing tissue due to its mechanically compliant, configurable and multi-modal design.

I. INTRODUCTION

The impact of soft robots has been seen throughout the medical field, e.g., in assistive technologies and rehabilitation [1], minimally invasive surgery [2], implants [3], and wearables [4]. One of the main advantages of soft robots is their compliance, enabling safe interaction with the human body and thus, increasing the wearability of technologies for the treatment of various clinical conditions.

Tissue repair, in particular, can benefit from the characteristics of soft robots, such as gentle dexterous handling, palpation, anatomical and functional support. Advanced surgical tools, e.g., Da Vinci robots, have demonstrated the benefit of added accuracy and minimizing invasiveness to the surgical procedures for tissue repair. However, they require surgeon supervision during the surgery, but provide no further control of the tissue repair beyond the surgical intervention. Alternatively, tissue engineering aims to restore the structure and function of a tissue by stimulating cells to proliferate on scaffolds using chemical growth factors [5]. Despite advances in structural tissue regeneration, tissue engineering faces challenges such as lack of vascularity in new tissue, poor mechanical compatibility, and lack of control of the regeneration process after the scaffold implantation [6].

¹Department of Automatic Control and Systems Engineering, University of Sheffield, UK. d.damian@sheffield.ac.uk [†]EPG and JJ contributed equally. Support for this work has been provided by the University of Sheffield and The National Council of Science and Technology of Mexico.

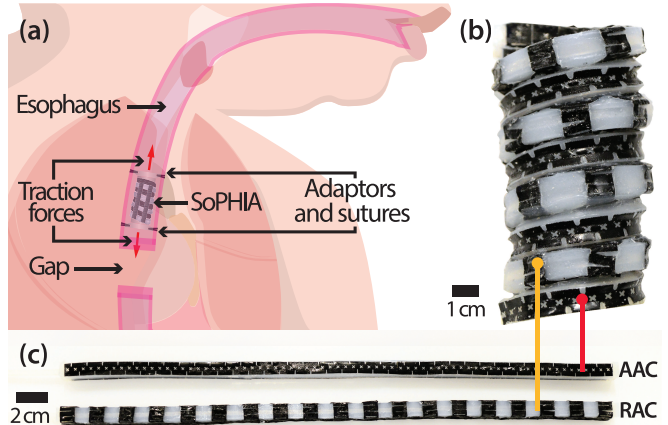


Fig. 1. The soft helical actuator for mechanostimulation-based tissue regeneration. (a) The envisaged implantation of SoPHIA inside the esophagus to treat the long-gap condition. It may be attached to the tissue by using sutures or adaptors [7]. (b) A view of the helical actuator made by configuring two actuation chambers. (c) The two chambers, axial (AAC) and radial (RAC) before the helical configuration to stimulate the tissue axially and radially respectively [8].

Mechanotherapy has been found to have assistive and therapeutic effects for a variety of medical conditions [9], including tactile sensory restoration [10], wound healing [11], regeneration of skeletal muscle and esophageal tissue [12], bone growth and skin grafts [13], [14].

Robotic implants are a new medical technology with the potential to unify the advantages of mechanical stimulation to tissue repair and regeneration, by exploiting the cells’ intrinsic proliferation mechanisms. They also have the potential to engineer and control the process of tissue repair, brought by medical devices, robots and surgical assistance, during the entire duration of treatment via remote communication [15]. These regenerative implants may be deployed inside the body and be mounted on the target tissue. There, they will exert controlled and gentle forces, and elongation on the tissue to induce regeneration and healing.

An example of potential therapies in which robotic implants may be of use is the regeneration of the gastrointestinal (GI) tract. This type of regeneration is required for conditions such as long-gap esophageal atresia (LGEA) (Fig. 1 (a)) or short bowel syndrome (SBS), congenital conditions in which more than two-thirds of these organs may be missing [16], and for which current treatments prove suboptimal with high mortality rates [17]. Our group recently introduced a robotic implant that was able to induce growth of esophageal tissue

using mechanostimulation and showed 77% of tissue growth over nine days [12]. This rigid implant was mounted on the esophagus and gently pulled the tissue axially. It was able to apply traction forces in the range of 1-2.5 N and displaced up to 5 cm of tissue [3].

Despite the potential of these robotic implants, the *in vivo* studies also revealed a range of unanticipated challenges due to the fixed design of the implant operating long-term in a harsh *in vivo* environment. Given the interaction between the rigid implant and the tissue, we ascertained that tissue scar level was significant, 37% of the new tissue, because of collagen formation.

The derived requirements for mechanostimulation-based robotic implants for tissue regeneration are: (1) mechanical compliance to reduce inflammation [18]; (2) minimally invasive implantation by surgeons in various parts of the GI tract; (3) a design that allows hyperelastic linear deformation while securing anti-buckling structural strength to resist considerable loading; (4) safe control of the delivery of mechanical stimulation.

To address these requirements, we introduced the concept and fabrication of a Soft Pneumatic Helically-Interlayered Actuator (SoPHIA). This multi-modal soft actuator is composed of two pneumatic chambers coiling together into a tubular implant for mechanotherapy tissue regeneration (Fig. 1 (b-c)) [8]. Due to its helical arrangement and reinforced walls, the soft helical actuator is capable of both axial elongation and radial expansion to stimulate the growth and function of the longitudinal and circular muscles of the GI tract. In this work, we present a holistic characterization of the soft actuator's capabilities in the axial, radial, and combined actuation mode, a simulation using a novel *in vivo* tissue growth simulator, as well as the control of SoPHIA.

II. RELATED WORK AND DESIGN REQUIREMENTS

The clinical requirements mentioned in the previous sections translate into a number of technical requirements. First, the actuator should be soft to mechanically comply with the target tissue. Recent studies in material engineering and tissue regeneration suggest that mechanically compliant implants [18] and the application of mechanotherapy may reduce the inflammatory response of the body [19]. Soft-matter robotic implants would thus be a suitable choice for mechanotherapy-based tissue repair.

Second, the actuator should be modular, to facilitate implantation, and configurable, to allow its mounting on tubular tissues in a non-invasive or minimally invasive manner. Soft actuator research has generally focused on pre-programmed axial lengthening and bending actuation based on fluidic control, for navigation in surgical applications or for exoskeletons [20]. Advances have been made towards modular soft robots for assistive applications [21]. Such devices are highly desirable for non-invasive surgery and implantation as well, yet have not been tested for their reliable extension under sustained loading conditions, as required for mechanostimulation. More recent work has also explored the strength of these actuators with programmable composites,

demonstrating the exertion of axial forces to lift up to 1kg after being pressurized at 23.8 kPa, and the expansion of more than 200% their original size [22]. However, the actuator has a large volume due to its origami creases, which is not desirable for an implant that seemingly coats a tubular tissue. While soft medical devices and implants have been recently proposed [23], more work needs to be done to reduce the implantation invasiveness.

Third, the actuator should elongate with the growing tissue without buckling due to load from the tissue or the body's spatial constraints. As soft actuators' directional expansion needs to be increased, to support large tissue reconstruction, it is critical to have actuators that maintain structural strength and do not buckle under load. The compliance of soft robots is limiting in this regard, making it challenging for them to withstand forces from their environments [24].

Helical or coiled structures are widely found, in both biology and engineering, due to their ability to handle tension and compression [25], or to provide enhanced maneuverability and stability, for example to endoscopic instruments [26].

When used in soft robotic systems, they also provide increased dexterity, more efficient workspaces by using routed tendons [27], enhanced area of contact and stability when acting as a gripper [28]. Nevertheless, scarce attention has been put into their investigation.

Fourth, a control of the actuator similar to the current clinical treatment is needed. In general, it is difficult to develop accurate models and control of soft actuators [29] due to the diversity in hyperelastic-based material constituents. Recent research has developed a variety of new methods for control, capable of dealing with the increased dimensionality and complexity [30]. One common approach for bending linear soft robots is derived from piecewise constant curvature modeling, based on which classical control strategies can be employed [31]. Despite the promising results, for more complex soft robots, the method is often ill-suited, as the dynamic behavior with the environment is not captured. Apart from these typical problems, overcoming the soft actuator's reliable extension under loading adds new challenges, such as buckling and undesirable bending. Given the gap in control strategies for complex soft robots, we used one of the common approaches of outsourcing some of the control to the robot's morphology and design [32].

In this paper, we embed the aforementioned requirements in a helically configurable soft pneumatic actuator that applies controlled multi-modal mechanostimulation. We introduce the following contributions to this area of research: (1) introduction of the concept of coiling soft assembly for realizing deployable, multi-modal, compact, soft yet strong, and adaptable soft robotic implants; (2) modeling and mechanical characterization of a soft helical actuator for axial elongation and radial expansion to deliver mechanostimulation to tissue; (3) a physical *in vivo* simulator of the biological tissue's stiffness and growth to allow for the evaluation of the helical actuator's performance; (4) a model-based multi-stage control of the axial elongation of the helical actuator according to tissue's physiological response.

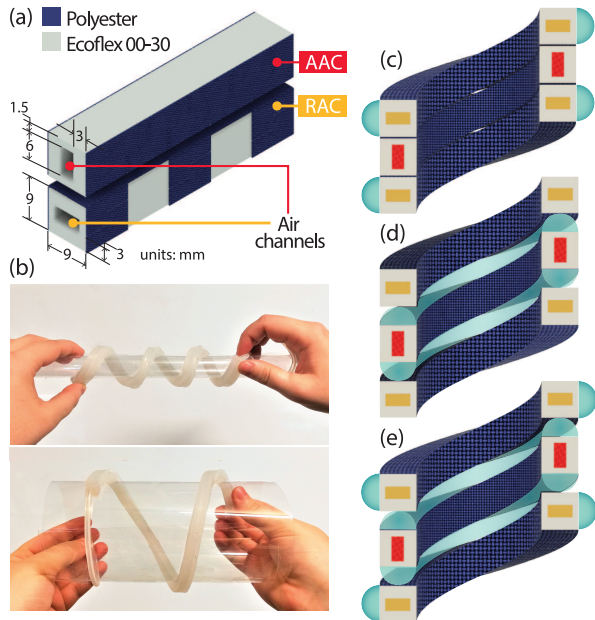


Fig. 2. SoPHIA Design. (a) Pneumatic chambers with embedded polyester that constraints inflation. (b) The pneumatic chambers can be configured into a helix around structures of varying diameter. (c) Cross-sectional area of SoPHIA when the RAC is inflated. (d) Cross-sectional area of SoPHIA when the AAC is inflated. (e) Cross-sectional area of SoPHIA when both chambers are inflated.

III. SOPHIA'S CONCEPTUAL DESIGN

We designed a soft actuator that is based on the anatomy of the GI tract. Most of the GI tract presents two types of muscle layers with fibers oriented circularly and longitudinally [33]. Therefore, a soft actuator for these organs should apply traction forces to both ends of the muscle layers in order to optimize the quality of the engineered tissue.

SoPHIA is an entirely soft actuator, made out of two identical elastomeric pneumatic chambers; the axial actuation chamber (AAC) and the radial actuation chamber (RAC) (Fig. 2(a)). Each chamber has a length of 48 cm, reaching 10.7 cm of height when the chambers are helically arranged and unpressurized. SoPHIA has a total weight of 95 grams. The chambers are made of Ecoflex 00-30 (Smooth-on Inc.) and can be configured into a helix of different diameters, depending on the tubular organ where it is placed (Fig. 2(b)). They are wrapped in polyester fabric, which in the AAC restricts radial expansion, while in the RAC restricts axial elongation (Fig. 2(c-e)). The AAC expands to displace adjacent chambers, increasing the axial size of SoPHIA. The RAC exhibits laterally emerging balloons from the unconstrained sections, yielding radial expansion. These chambers are coiled together into a helical structure with interlayered actuation (Fig. 2(e)) (Fig. 1(b-c)). Details of the conceptual design, fabrication and Finite Element Modeling of the chambers are in [8]. Details on SoPHIA's fixation to *ex vivo* esophagus tissue are described in [7].

IV. SOPHIA'S ANALYTICAL MODEL

In this section, an analytical model of the helical actuator is introduced and validated, to understand the relation

between the physical components and their mechanical response to pressurization.

A. Analytical model

For simplicity, the model is separated into two parts, one model for the AAC and one for the RAC. The main performance metrics are elongation and expansion. At equilibrium, the force balance equations projected respectively on \mathbf{e}_x and \mathbf{e}_r (Fig. 3) can be written as:

$$P_x S_x - F_{ex} - F_t = 0 \quad (1)$$

$$\int_{\theta_1}^{\theta_2} h P_r R d\theta - \int_{\theta_1}^{\theta_2} w \sigma_{er} R d\theta = 0 \quad (2)$$

where F_{ex} denotes the resistance force of the elastomeric walls to expansion along \mathbf{e}_x , F_t is the resistive force of the host tissue during the mechanotherapy treatment, P_x and P_r are the relative pressure of the air inside the air channels of the AAC and the RAC respectively. S_x is the cross-sectional area of the air channel of the AAC, h denotes the height of the air channel of the RAC, w is the thickness of the RAC walls and R is the external radius of the RAC, σ_{er} is the elastic stress of the elongated wall in the radial expansion of the robot, θ_1 and θ_2 are the angular limits of the area considered for the force balance equation, and finally $d\theta$ is the angular differential for the integration.

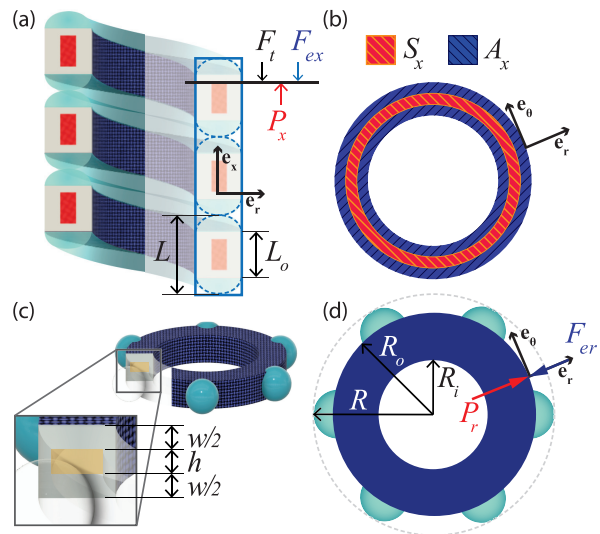


Fig. 3. Model of the simplified (a) side-view and (b) top-view axial elongation showing the interacting forces and areas respectively. (c) Perspective cross-sectional area and (d) top-view radial expansion showing the lengths and interacting forces respectively.

We made the assumption that the two chambers can be decoupled and act independently in a single direction and that they deform uniformly. To simplify the analysis, we assumed that the coiled chambers behave as a stack of N circular chambers. The weight of the actuator and the weight of the air are neglected. Finally, we neglect any possible radial force applied by the tissue to the robot in order to match the characterization test presented in section V.

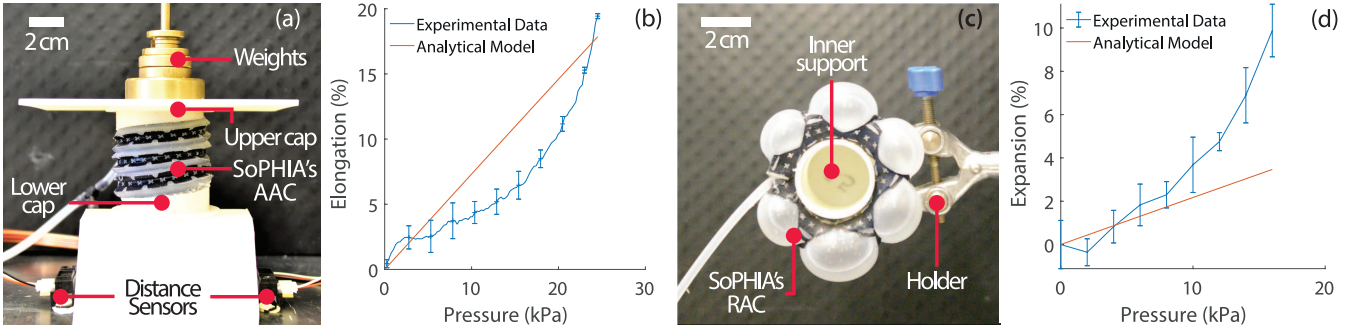


Fig. 4. Experimental validation of the mathematical model for SoPHIA's actuation chambers. (a) Side view of three AAC pressurized SoPHIA coils used to validate the mathematical model of axial inflation. (b) Experimental and analytical evaluation of the AAC actuation. (c) Top view of one of the RAC pressurized SoPHIA coils used to validate the mathematical model of radial inflation. (d) Experimental and analytical evaluation of the RAC actuation. Error bars stand for standard deviation of 3 trials. We pressurized the samples from 0 to 25 kPa for the AAC and from 0 to 22 kPa for the RAC. For the AAC, we used 2 N of load to represent the resistive force of the host tissue [12]. For the RAC, the resistive force was not considered.

Silicone rubbers are known as hyperelastic materials. Using a Neo-Hookean model for incompressible material in a uniaxial elongation to describe the elastic behavior of the chambers walls, equations (1) and (2), respectively, can be rewritten as follows:

$$A_x \frac{2E}{6} \left[\left(\frac{L}{L_0} \right)^2 - \frac{L_0}{L} \right] + F_t = S_x P_x \quad (3)$$

$$w \frac{2E}{6} \left[\left(\frac{R - R_i}{R_0 - R_i} \right)^2 - \frac{R_0 - R_i}{R - R_i} \right] = h P_r \quad (4)$$

A_x is the cross-sectional area of the elongated material in the AAC, E is the Young's modulus of the material, L is the height of the AAC after elongation, L_0 is the initial height of the AAC, w is the width of the elongated material in the RAC, R , R_i , and R_0 are respectively the external radius of the RAC once elongated, the internal radius of the RAC, and the initial external radius of the RAC. Fig. 3 illustrates the main parameters considered in the model.

The model parameters are given in Table. I. In order to estimate the Young's Modulus, we used least squares curve fitting using the axial elongation results with the model obtained in equation (3). The Young's modulus was optimised in the range of values found in the literature, from $E = 0.027$ MPa [34] to $E = 0.069$ MPa [35]. After the fitting, the best Young's modulus was determined to be $E = 0.068$ MPa. The values in Table. I are based on the geometry of the actuator. The value for the resistance force F_t was taken from [12].

B. Experimental validation of the model

Two experiments were run to validate the analytical model derived in the previous section. To validate the analytical model for the AAC, we coiled three turns of that chamber around an oiled (Cole Parmer VacuumPump Oil CP 500) PLA tube to reduce friction and support it vertically without restricting its movement (Fig. 4(a)). An ABS plate at the top of the AAC acted as a reference for the two reflective distance sensors (GP2Y0A41SK0F, Sharp) to measure the elongation, as well as to support the weights that simulate the

TABLE I
MODEL PARAMETERS

Notation	Description	Value	Unit
S_x	cross-sectional area of the inner channel of the AAC	415	mm ²
A_x	cross-sectional area of the elongated material in the AAC	829	mm ²
w	width of the elongated material RAC	6	mm
h	height of the RAC air channel	3	mm
R_0	initial external radius of the RAC	2.49	mm
R_i	internal radius of the RAC	17.5	mm
L_0	initial height of the AAC	9	mm
F_t	resistive force of the host tissue during the mechanotherapy treatment	2	N

resistive force F_t . We used two distance sensors, averaging the readings, in order to avoid inaccuracies due to uneven elongation of the actuator on either side. We pressurized the AAC from 0 to 25 kPa and recorded the elongation readings to obtain L . We performed three trials. For the experiments, we define elongation as $\frac{L-L_0}{L_0}$.

To validate the RAC, we glued one turn of the RAC, along its entirely constrained face, around an ABS tube using cyanoacrylate adhesive (Fig. 4(c)). The ABS tube was supported by a clamp stand. Then, we pressurized the RAC from 0 to 20 kPa and measured its radial expansion, defined as $\frac{R-R_0}{R_0}$ over three trials using ImageJ (NIH).

For both chambers, relative pressure was considered. The maximum pressure values were defined considering pressurization before anisotropic deformation and failure.

As can be seen in Fig. 4(b) and Fig. 4(d), there is a reasonable agreement between the theoretical models and the experimental values. The Root Mean Square Error (RMSE) between the three AAC elongation trials and the analytical model are 2.5%, 2.9%, and 3.6%. This means that on average, the error taken by using the model instead of the real data is 3.0 percentage points of elongation. The RMSE between the three RAC elongation trials and the model are 3.0%, 2.1%, and 3.2%; in this case the average error is

2.8 percentage points of expansion. The RMSE over trials shows that the error made per trial is consistent. The average error is similar for the two chambers but their ranges of expansion are different. Since the AAC has a longer stroke, the normalized standard error is smaller than for the RAC.

The observed differences, in both the AAC and the RAC, can be explained by the model limitations. First, the proposed model only takes into account the wall elongation in one direction during the pressurization, but does not consider the ballooning behavior of the chambers. Secondly, the Neo-Hookean model was chosen for its simplicity, in order to provide information about the impact of each design parameters, e.g., size, Young’s modulus, on the actuator’s elongation for a potential adaptation of SoPHIA to other applications.

V. SOPHIA CHARACTERIZATION

We conducted experiments to characterize SoPHIA’s elongation, expansion and force capabilities, to determine both its standalone capabilities, as well as those under conditions that are expected clinically. This section describes the corresponding experimental setups and methods. The electronic control platform is described in [8].

A. Axial Elongation

Considering that SoPHIA’s primary application is to elongate tissue via mechanostimulation, it is relevant to characterize its axial elongation in dynamic conditions in order to evaluate its suitability to elongate tissue. In this set of experiments, we investigated the hysteresis of SoPHIA by measuring the free-load axial elongation response of the AAC, the RAC and the simultaneous pressurization (AAC+RAC) to pressures of 25 kPa, 20 kPa and a combined 55 kPa respectively. These were pressurization cycles of 2 seconds.

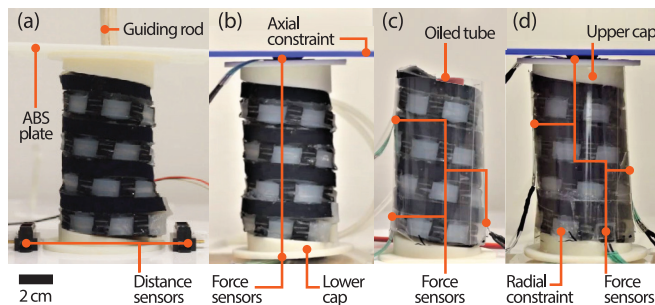


Fig. 5. Experimental setups to characterize elongation, expansion and force capabilities. (a) SoPHIA placed around an oiled tube and a rod that guides the axial freeload elongation of an ABS plate to record the actuator’s elongation. (b) Two force sensors were placed at the top and bottom of an axially restricted SoPHIA to measure axial forces. (c) Three force sensors were placed on the expandable sections of the RAC to record forces exerted against a PET sheet that envelops SoPHIA. (d) SoPHIA restricted axially and radially to record overall forces.

We placed SoPHIA around an oiled (Cole Parmer Vacuum Pump Oil CP 500) plastic tube to reduce friction and support it vertically without restricting its movement. A rod guided

the axial elongation of an ABS plate that worked as a reference to the distance sensors to measure SoPHIA’s elongation (Fig. 5 (a)). This rod was necessary for the benchtop tests, yet not needed for the clinical setting when SoPHIA will be fixed to the tubular tissue. We performed three trials of five cycles each. Then, we inflated the AAC+RAC up to their breakage point to find their maximum expansion before failure, leaving time to settle. For this experiment, we only needed the oiled tube to support the actuator under free-load conditions (Fig. 5 (a)). The elongation was recorded and then measured using ImageJ (NIH).

B. Axial and Radial Output Forces

Given that SoPHIA may be used as an implantable device, it is necessary to understand the potential forces that it can exert against the target tissue. According to [12], forces to stretch the tissue axially should be around 2.3 N. In order to investigate if this force requirement is fulfilled, and considering the interdependence of the AAC and the RAC found in our previous work [8], we proceeded to characterize the force interactions between the two chambers under constrained and unconstrained setups, performing five trials for each set of conditions.

To measure the axial forces exerted by SoPHIA’s elongation, we placed two force sensors on the top and bottom of the actuator respectively, and we restricted its expansion in these same two locations as shown in Fig. 5 (b). Both force sensors were averaged to get an overall reading of the maximum axially exerted force. Then, we pressurized the AAC and the RAC independently and simultaneously. The constraints were placed in direct contact with SoPHIA. To measure the radial forces exerted by SoPHIA’s expansion, the actuator was enveloped in a rigid polyethylene terephthalate (PET) cylinder with force sensors adhered to its inner surface and in direct contact with the unconstrained segments in the RAC, as shown in Fig. 5 (c). Then, we pressurized the AAC and the RAC independently and then simultaneously. To measure the overall forces that SoPHIA can exert, the actuator was constrained both axially and radially at the same time (Fig. 5 (d)). Then we pressurized the AAC and the RAC independently and then simultaneously.

C. Structural Strength

Since SoPHIA needs to sustain forces over a long period of time, structural strength is an important feature to test, to determine how much weight the implant can support, at different inflation levels, without buckling. To test the structural strength, both the axial and radial chambers were inflated at 3 different levels of averaged pressure - 10.5 kPa, 13.5 kPa and 16.5 kPa - as well as non-inflated. With no constraints around SoPHIA, weights were then progressively added, until we observed the actuator buckling. The weights were guided on to the top cap of SoPHIA by an acrylic tube. We repeated the experiment five times.

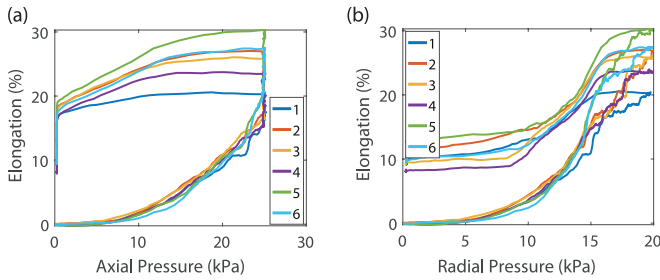


Fig. 6. SoPHIA's dynamic elongation behavior. (a) Elongation behavior as a function of axial pressure and (b) as a function of radial pressure when the AAC and the RAC are simultaneously actuated. SoPHIA exhibits hysteresis behavior and yields up to 30% of freeloading axial elongation under pressurization cycles of 2 seconds. Experimental conditions are detailed in Section V-A.

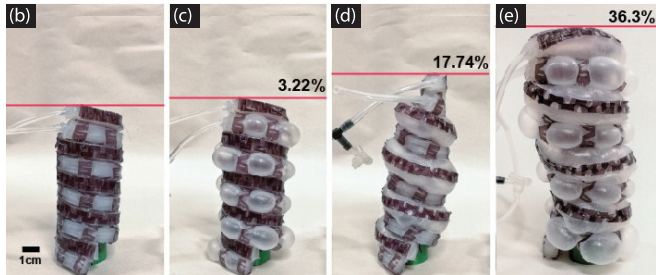


Fig. 7. SoPHIA's static behavior under different actuation modes. (a) SoPHIA in a relaxed state, (b) with only the RAC inflated, (c) only the AAC chamber inflated and (d) both chambers inflated. By inflating the AAC (25 kPa) and the RAC (20 kPa) simultaneously, SoPHIA is capable of reaching 36.3% of elongation in comparison to its original size.

VI. RESULTS

A. Axial Elongation

Under dynamic conditions, with two-second cycles, SoPHIA can axially elongate 0.25 cm at 25 kPa when only the AAC is pressurized, 0.7 cm at 20 kPa when only the RAC is inflated and 2.8 cm when both are pressurized simultaneously (Fig. 6). The elongation capability is enhanced by simultaneous pressurization of the chambers, exhibiting nonlinear and hysteresis behavior. In comparison, under static conditions (when the actuator had time to settle) SoPHIA can axially elongate 3.2%, 17.7% and 36.3% of its original size when the RAC, the AAC and RAC+AAC are actuated respectively (Fig. 7).

B. Axial and Radial Output Forces

SoPHIA is capable of exerting up to 7 N axially, when the AAC and the RAC are pressurized simultaneously at 38 kPa while entirely constrained (Fig. 8(c)), and it only exerts 0.69 N radially under the same conditions (Fig. 8(d)). This behavior is constant along all the setups, meaning that SoPHIA tends to direct its forces 90% more axially than radially. This is confirmed by looking at Fig. 8(a) and (b). This result is positive considering the intended clinical application as it means that SoPHIA is capable of exerting higher forces than the ones needed in proved functional mechanotherapy [12] at low levels of pressure. SoPHIA can exert up to 1.35 N of force at 38 kPa when it is radially

constrained which is equivalent to the force we would be able to yield against a tubular organ (Fig. 8(b)).

C. Structural Strength

SoPHIA's helical configuration provides increasing structural strength, with increasing levels of average pressure. In a relaxed state, SoPHIA can stand 500 g of weight without buckling (Fig. 9(a)). This strength increases as the actuator increases its inner pressure. Pressurized at an average of 16.5 kPa, it can withstand up to 800 g (Fig. 9(b)).

VII. SOPHIA STAGED CONTROL

After characterizing SoPHIA, the control requirements for the real-life application were considered. Envisaging the *in vivo* tissue growth treatment, SoPHIA will be fixed at its ends inside the tubular organ and will inflate axially every 24 hours in order to apply tension to the tissue. During the week-long traction procedure, the physiological response of the tissue stiffening is to resist to the applied traction forces [16]. A release of this tension can be observed on the tissue between the traction applications, as a consequence of tissue relaxation and growth. In this section, we describe the setup, experimental procedure, results and SoPHIA's control used to simulate staged tissue growth mechanotherapy.

A. Tissue Growth Simulation

1) *Physical Simulator*: A benchtop tissue growth simulator, shown in Fig. 10, was developed in order to derive the control of SoPHIA in an environment similar to the one *in vivo*. The benchtop simulator has two roles: to simulate the tissue stiffness and growth, and to monitor SoPHIA's performance. The tissue growth and stiffness are simulated via two mechanisms: a passive spring actuated plate, and a controlled lifting plate. Monitoring is then achieved using pressure, force and distance recordings from the platform.

Tissue growth and stiffness were simulated using a combination of passive and active mechanisms. The tissue stiffness is replicated using a compression spring (LP 026LM 06S316, Lee Springs) - which has a 0.05 N/mm spring rate, 50.8 mm free length, 7.035 mm solid length. As SoPHIA lengthens it experiences a resistant force corresponding to the level of spring compression. The spring itself was mounted around a plastic rod capped by two acrylic plates to prevent buckling.

The tissue growth was achieved using the active mechanism, made up of two NEMA-23 stepper motors (57STH56, Phidgets), controlled by two stepper motor drivers (TB6600, TopDirect) through an Arduino Uno R3 microcontroller. The two motors are coupled to two vertical M8 threaded bars which lift the moving plate. The moving plate itself carries the passive spring mechanism and, when displaced vertically, allows the spring to decompress, thus simulating tissue growth. The tissue growth is monitored via two distance sensors which measure the displacement of the moving plate.

Throughout the simulation, SoPHIA is also monitored by three different sensor readings: pressure, force and distance. The pressure recordings are taken from the dedicated AAC and RAC PCBs. Similarly to the previous experiments, the

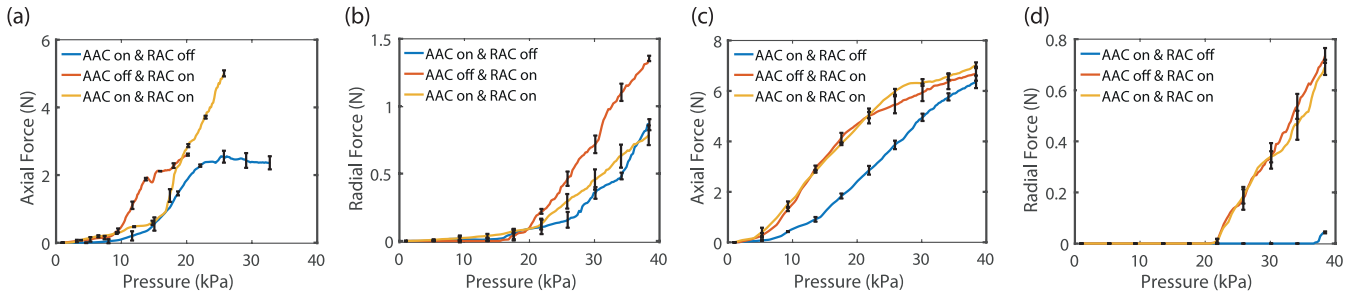


Fig. 8. Mean output force capabilities with standard deviation for five trials. (a) Axial forces under axial constraints and three actuation modes. (b) Radial forces under radial constraints and three actuation modes. (c) Axial forces under axial+radial constraints and three actuation modes. (d) Radial forces under axial+radial constraints and three actuation modes. As expressed in the results section, axial forces represent the most benefited from interdependence between chambers with the lowest standard deviation among trials and conditions. Experimental conditions are specified in Section V-B.

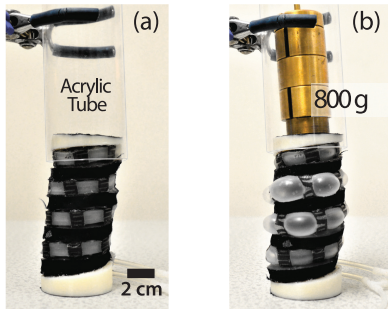


Fig. 9. SoPHIA's structural strength demonstrated (a) in a relaxed state and (b) at an averaged pressure of 16.5 kPa withstanding a maximum weight of 800 g.

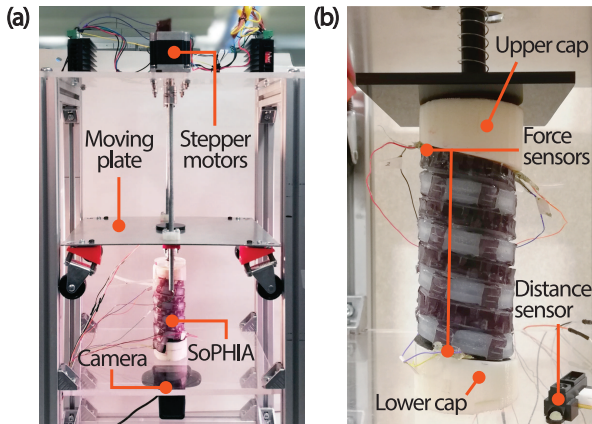


Fig. 10. Physical simulator of tissue stiffness and growth. (a) Overall side view; (b) detail of the sensors and actuator in the physical simulator.

force recordings are taken from four force sensors, two placed on the top and two placed on the bottom. SoPHIA's elongation is measured by taking the average of two distance sensors which track the displacement between the spring actuated plate and the ground plate.

2) *Experimental Procedure*: We simulated the growth of 3.2 cm of virtual tissue by expanding SoPHIA axially, inflating simultaneously the AAC and the RAC. The elongation of both chambers was semi-constrained by the spring actuated plate, in order to simulate the resistance that SoPHIA will experience from the tissue under stretch. SoPHIA was

constrained by a PET sheet, simulating its enclosure in a tubular tissue shown in Fig. 11(a). Both chambers were pressurized simultaneously, controlled by the target distance determined for each stage, shown in Fig. 11(a-e). The overall target distance of 3.2 cm was chosen as the maximal semi-constrained inflation elongation before risk of failure.

The procedure followed for the simulation of tissue growth consists of four stages described in Fig. 11. Firstly the actuator is inflated and then the moving plate is lifted to decompress the spring mechanism. Using this procedure, two sets of experiments were performed. The first set consisted of using manually tuned values for each stage that were then further improved in the second set using modeling and automatic tuning. Each set of experiments consisted of five trials. In this setup, SoPHIA exerts up to 0.19 N of force before decreasing as a result of the upwards displacement of the moving plate, simulating tissue relaxation at the end of each stage (Fig. 12). These results match with the previously stated experimental protocol in Fig. 11(a-e). The initial interaction force between SoPHIA and the tissue simulator was set to around 0 N, although could be tuned to other values depending on the initial position of the moving plate relative to SoPHIA.

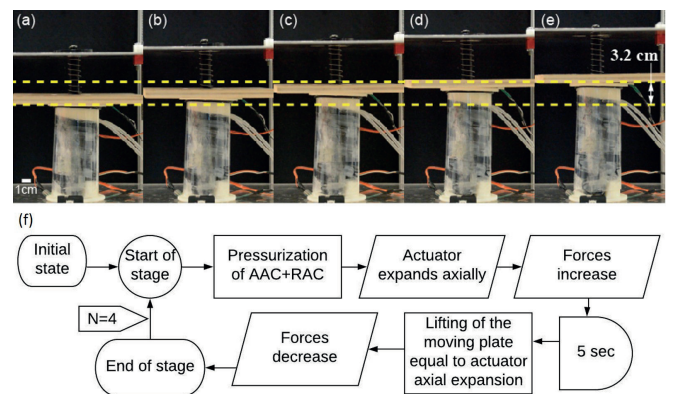


Fig. 11. Experimental procedure for the simulation of tissue growth treatment based on the staged application of traction forces. The dashed yellow lines represent the initial and final states of the moving plate. (a) SoPHIA in a relaxed state; (b) end of stage 1 reaching 0.8 cm, (c) end of stage 2 reaching 1.6 cm, (d) end of stage 3 reaching 2.4 cm, and (e) end of stage 4 reaching 3.2 cm. (f) Flowchart describing each stage in the simulation.

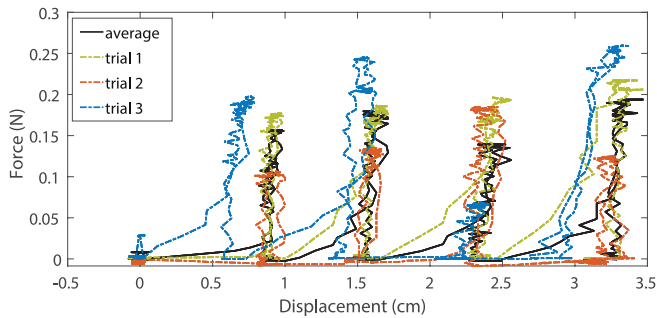


Fig. 12. Force response of SoPHIA caused by its elongation. The decrease in force represents the end of each of the stages during the simulation.

B. Modeling and Control for Axial Elongation

In this section, the control details of SoPHIA’s axial elongation in the tissue growth simulator are explained. The requirements of the controller are first established and more details about the controller used are given. The modeling approach is then presented, detailing how the transfer function models are derived. Finally, the control tuning is described and compared against the initial requirements.

1) *Specifications*: To establish the requirements for the controller design, both the clinical requirements and the current limitations of the actuator were taken into account. A steady-state error requirement of less than 1mm was set. The steady-state error was limited to 1 mm, to be as small as possible, while taking into account the precision of the distance sensors that is around ± 1 mm. In addition, the rise time was set to be maximized to ensure a slow elongation of the tissue and to avoid tearing.

For the system itself, a position PI controller was used, as it was deemed appropriate to meet the requirements. A target elongation of 0.8 cm for each stage was chosen, to have 4 stages of visually noticeable elongation. Additionally, an overall safe pressure limit of 39 kPa was enforced, and stopped inflation if reached, to ensure SoPHIA would not burst. This overall safe pressure limit was determined from the maximum pressure of the previous experiments. Based on these design requirements and inspired by the current daily clinical intervention for tissue elongation [16], a gain-scheduled lengthening process was hypothesized to be suitable. Gain-scheduling was chosen to allow for better tracking of the reference signal and improve the overall behavior of the actuator. The PI values for all of the stages were initially set based on testing of previous actuators, before being improved later based on the modeling.

2) *Modeling*: For each of the stages, a model was found using system identification to aid with the tuning of the PI controller. Based on the linear dynamics observed in each stage, a low order linear time invariant transfer function was fit to the data. Of the five trials conducted, the best trial, selected based on minimal overshoots and minimal steady-state error for each stage, was chosen for modeling. A model was fit to this selected trial, identifying a second order model for stage 1 and first order models for the remaining stages. The transfer functions were determined

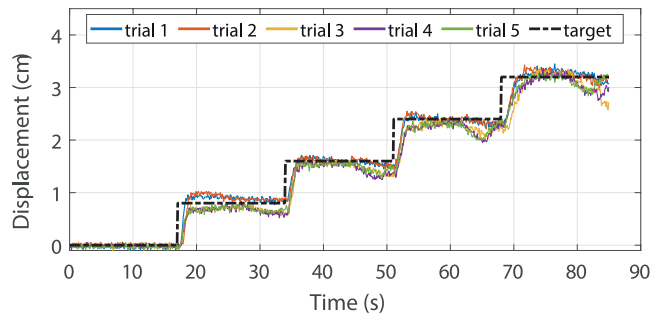


Fig. 13. Plot of all of the trials with the improved control throughout all 4 stages.

using subspace identification with an automatic estimation of the initial condition and using the instrument variable approach for initialization.

3) *Control*: The PI values for each of the stages were tuned to meet the requirements set out in section VII-B.1. The overall aim of the tuning process was to achieve a smaller steady-state error, while keeping rise time as slow as possible. The digital tuning of the PI values was done using the Ziegler-Nichols method applied to the developed model transfer functions. For the tuning, a small steady-state error was prioritized, as well as a slow rise time to achieve a steady inflation. After this initial digital tuning, the PI values were then further fine-tuned, taking into account the noticed behavior changes to smooth the response. Fig. 13 shows the comparison between initial and improved control throughout all 4 stages, where we demonstrate an improvement by implementing automatic tuning on the gain-scheduled lengthening process control scheme. The averaged achieved performance from the first five trials and the next five trials with improved control are summarized in Table. II.

Overall, most of the stages showed a decrease in steady-state error or at least comparable values with the improved control, although this did come at the cost of greater overshoots and faster rise times. Additionally, compared to the initial tunings, where rise times were not available for stages 1 and 4 as 90% of the target value was not reached, all of the stages with the improved control reached these target values as a minimum. Overall, the system met the requirement of a steady-state error of less than 1 mm across all stages, promising safe operation for the envisaged clinical procedure.

VIII. DISCUSSION & CONCLUSION

We introduced a Soft Pneumatic Helically-Interlayered Actuator (SoPHIA), capable of configurability and multi-modal axial elongation and radial expansion, that we envisage as an implantable device to provide mechanostimulation for tissue growth. We evaluated SoPHIA’s performance using a novel physical simulation platform that we envisage to be used as a research tool for tissue regeneration simulation.

We tested the capability of this actuator by evaluating the elongation, output force and characterizing its nonlinear behavior. SoPHIA is capable of growing axially 36.3% its

TABLE II

AVERAGED PERFORMANCE CHARACTERISTICS FOR THE INITIAL AND IMPROVED TRIALS. TR: RISE TIME, OS: OVERSHOOT AND SSE: STEADY-STATE ERROR.

	Initial				Final			
	Stg1	Stg2	Stg3	Stg4	Stg1	Stg2	Stg3	Stg4
Tr (s)	x	4.05	3.30	x	1.12	1.20	1.90	2.45
OS (%)	0	0.25	1.50	0.44	11.25	4.63	2.83	5.94
SSE (cm)	0.11	0.05	0.04	0.09	0.07	0.02	0.05	0.07

original size under freeload static conditions at an average pressure of 22.5 kPa and 33.3% under loaded-staged control at an average pressure of 21 kPa. By constraining SoPHIA entirely and then pressurizing both chambers, which is a clinically-realistic condition, SoPHIA can exert up to 7 N axially and up to 1.35 N radially, if only the RAC is pressurized. These capabilities make the actuator suitable to address the reconstruction of tissues in clinical conditions such as LGEA (where more than 3 cm of tissue is missing) or SBS.

While the output performance of the soft actuator is comparable to many soft pneumatic actuators [36], [21], the design and behavior of SoPHIA provide unique features that are clinically advantageous:

- By using a geometrically simple building block (actuation chambers) that can be coiled from one to a three-dimensional actuator, we can configure SoPHIA into a cylinder that fits to various diameters of hollow organs and tubular tissues, making it a versatile medical tool.
- Its ease of configuration could facilitate clinical intervention on different organs. This potentially could be done by performing a small incision near the target organ, through which the AAC and RAC could be inserted, implanted and removed employing minimally invasive surgery procedures such as laparoscopy.
- By varying the orientation of the chambers, we can address different conditions. For example, the RAC could be oriented to expand inwards in order to stimulate the intestine during SBS treatment. It can also be oriented to expand outwards during LGEA treatment (Fig. 1).
- The helical shape also provides structural support, with air pressure distributed uniformly across the diameter and height of the actuator. We showed that the implant can support up to 800 g without buckling. This feature is clinically important as buckling could lead to a misshaped organ.

Over the duration of the treatment, the AAC may be progressively inflated to support the lengthened tissue. The RAC may be intermittently inflated to provide radial stimulation to the tubular organ and also decrease fibrotic response. Powering and monitoring a robotic implant via loose cabling that exits the body through a skin port into a control box was demonstrated clinically viable in [12]. For the pneumatic tubing a similar approach is envisaged, however this needs to be tested pre-clinically. As presented in our previous work [7], adaptors can be used to attach SoPHIA without being in direct contact with the organ to heal, in order to reduce fibrosis. SoPHIA's helical configuration provides

multi-modal behavior achieved by interlayering elastomeric chambers of different functions into the helix. Typically, soft helical actuators show some degree of torsion when they incorporate a backbone into their design [37]. SoPHIA is a zero-torsion helical actuator due to it being constrained axially and radially.

From the dynamic elongation tests, we observed that the RAC generates much more elongation than the AAC, whilst under static conditions the opposite is true. We hypothesize that this difference comes from the AAC having a much slower response time, partly caused by the stacking of coils. As the RAC showed superior dynamic expansion than the AAC, which is desirable for mechanotherapy, one option is to use the RAC design for axial inflation as well. Another alternative to increase SoPHIA's axial elongation is to decrease shear stress between the chambers caused by their different expansion rates that currently causes the actuator to burst.

We evaluated the behavior of SoPHIA using a novel physical simulator. During a week-long clinical tissue lengthening treatment, the tissue may become stiffer (due to inflammation), relax (due to its viscoelastic properties) or grow. These mechanical and physiological changes are being emulated by the physical simulator. Such simulations are difficult to achieve with current phantom tissues or with *ex vivo* biological tissues, as they exhibit limited lengthening. This makes the physical tissue growth simulator ideal to dynamically represent different states of tissues, from mechanical to metabolic, under either physiological or pathological conditions. Further work still needs to be done to simulate the radial growth, as well as the real-time stiffness variation of the tissue.

While the soft-matter actuator is desirable for its stretchability to support a growing tissue, its intrinsic nonlinear behavior needs to be precisely controlled for clinical safety. We thus developed a staged-position gain-scheduled controller, which emulates the daily tissue stretch within the existing clinical treatment. We successfully evaluated the implant control in a physiologically-relevant scenario. Variability of the system represents an important challenge when controlling it due to the sensor disturbances and elastomer non-linearity and wear. However, the presented analytical model constitutes a reliable tool for the prediction of the AAC and the RAC behavior, as there is a reasonable agreement between the theoretical models and the experimental values (Fig. 4(b) and Fig. 4(d)). Although the proposed model does not consider the ballooning behavior of the chambers, it provides qualitative information of the design parameters that impact SoPHIA's elongation. In the future other nonlinear models, such as Ogden, will be investigated in order to provide more detailed performance insights.

Due to the lack of kinematic equations that describe soft robots in general [31], our approach was a combination of using traditional control techniques and designing constraints to achieve the desired actuation. However, further research is still needed in order to model the behavior of soft machines from first principles. Consequently, we may be able to tune the controller better to decrease the steady-state error, while

keeping large rise times. Force control could also be used, such that SoPHIA applies constant traction forces and adapts to the tissue response.

Future directions include embedding soft sensors to record SoPHIA's elongation and forces, in order to carry out more accurate mechanotherapy control *in vivo*. Further work also includes the advancement of the axial elongation capability of SoPHIA for a larger capacity of tissue lengthening.

ACKNOWLEDGMENTS

We thank Manuela Garcia Hoyos and Margot Cobourg for their valuable help.

REFERENCES

- [1] L. N. Awad, J. Bae, K. O'Donnell, S. M. M. De Rossi, K. Hendron, L. H. Sloat, P. Kudzia, S. Allen, K. G. Holt, T. D. Ellis, and C. J. Walsh, "A soft robotic exosuit improves walking in patients after stroke," *Science translational medicine*, vol. 9, no. 400, 2017.
- [2] S. Miyashita, S. Guitron, K. Yoshida, S. Li, D. D. Damian, and D. Rus, "Ingestible, controllable, and degradable origami robot for patching stomach wounds," in *2016 IEEE International Conference on Robotics and Automation (ICRA)*. IEEE, 2016, pp. 909–916.
- [3] D. D. Damian, S. Arabagi, A. Fabozzo, P. Ngo, R. Jennings, M. Manfredi, and P. E. Dupont, "Robotic implant to apply tissue traction forces in the treatment of esophageal atresia," in *2014 IEEE International Conference on Robotics and Automation (ICRA)*, 2014, pp. 786–792.
- [4] Y.-L. Park, B.-r. Chen, N. O. Pérez-Arancibia, D. Young, L. Stirling, R. J. Wood, E. C. Goldfield, and R. Nagpal, "Design and control of a bio-inspired soft wearable robotic device for ankle-foot rehabilitation," *Bioinspiration & biomimetics*, vol. 9, no. 1, 2014.
- [5] A. Atala, F. K. Kasper, and A. G. Mikos, "Engineering complex tissues," *Science Translational Medicine*, vol. 4, no. 160, 2012.
- [6] R. Nigam and B. Mahanta, "An overview of various biomimetic scaffolds: Challenges and applications in tissue engineering," *Journal of Tissue Science & Engineering*, vol. 5, no. 2, 2014.
- [7] E. Perez-Guagnelli, J. Jones, and D. D. Damian, "Evaluation of a soft helical actuator performance with hard and soft attachments for tissue regeneration," in *Proceedings of the 12th Hamlyn Symposium on Medical Robotics*. The Hamlyn Centre, 2019, pp. 3–4.
- [8] E. R. Perez-Guagnelli, S. Nejus, J. Yu, S. Miyashita, Y. Liu, and D. D. Damian, "Axially and radially expandable modular helical soft actuator for robotic implantables," in *2018 IEEE International Conference on Robotics and Automation (ICRA)*, 2018, pp. 4297–4304.
- [9] C. Huang, J. Holfeld, W. Schaden, D. Orgill, and R. Ogawa, "Mechanotherapy: Revisiting physical therapy and recruiting mechanobiology for a new era in medicine," *Trends in Molecular Medicine*, vol. 19, no. 9, pp. 555–564, 2013.
- [10] D. D. Damian, A. H. Arieta, and A. M. Okamura, "Design and evaluation of a multi-modal haptic skin stimulation apparatus," in *2011 Annual International Conference of the IEEE Engineering in Medicine and Biology Society*, 2011, pp. 3455–3458.
- [11] L. Lancerotto and D. P. Orgill, "Mechanoregulation of angiogenesis in wound healing," *Advances in wound care*, vol. 3, no. 10, pp. 626–634, 2014.
- [12] D. D. Damian, K. Price, S. Arabagi, I. Berra, Z. Machaidze, S. Manjila, S. Shimada, A. Fabozzo, G. Arnal, D. Van Story *et al.*, "In vivo tissue regeneration with robotic implants," *Science Robotics*, vol. 3, no. 14, 2018.
- [13] C. Huang and R. Ogawa, "Mechanotransduction in bone repair and regeneration," *The FASEB Journal*, vol. 24, no. 10, pp. 3625–3632, 2010.
- [14] M. Daya and V. Nair, "Traction-assisted dermatogenesis by serial intermittent skin tape application," *Plastic and reconstructive surgery*, vol. 122, no. 4, pp. 1047–1054, 2008.
- [15] D. D. Damian, "Regenerative robotics," *Birth defects research*, 2019.
- [16] J. E. Foker, B. C. Linden, E. M. Boyle, and C. Marquardt, "Development of a true primary repair for the full spectrum of esophageal atresia," *Annals of surgery*, vol. 226, no. 4, pp. 533–43, 1997.
- [17] P. F. M. Pinheiro, A. C. S. e Silva, and R. M. Pereira, "Current knowledge on esophageal atresia," *World journal of gastroenterology*, vol. 18, no. 28, pp. 3662–3672, 2012.
- [18] P. Moshayedi, G. Ng, J. C. F. Kwok, G. S. H. Yeo, C. E. Bryant, J. W. Fawcett, K. Franze, and J. Guck, "The relationship between glial cell mechanosensitivity and foreign body reactions in the central nervous system," *Biomaterials*, vol. 35, no. 13, pp. 3919–3925, 2014.
- [19] C. A. Cezar, E. T. Roche, H. H. Vandenburg, G. N. Duda, C. J. Walsh, and D. J. Mooney, "Biologic-free mechanically induced muscle regeneration," *Proceedings of the National Academy of Sciences*, vol. 113, no. 6, pp. 1534–1539, 2016.
- [20] B. Mosadegh, P. Polygerinos, C. Keplinger, S. Wennstedt, R. F. Shepherd, U. Gupta, J. Shim, K. Bertoldi, C. J. Walsh, and G. M. Whitesides, "Pneumatic networks for soft robotics that actuate rapidly," *Advanced functional materials*, vol. 24, no. 15, pp. 2163–2170, 2014.
- [21] G. Agarwal, N. Besuchet, B. Audergon, and J. Paik, "Stretchable materials for robust soft actuators towards assistive wearable devices," *Scientific reports*, vol. 6, no. 1, 2016.
- [22] R. V. Martinez, C. R. Fish, X. Chen, and G. M. Whitesides, "Elastomeric origami: programmable paper-elastomer composites as pneumatic actuators," *Advanced functional materials*, vol. 22, no. 7, pp. 1376–1384, 2012.
- [23] E. T. Roche, M. A. Horvath, I. Wamala, A. Alazmani, S.-E. Song, W. Whyte, Z. Machaidze, C. J. Payne, J. C. Weaver, G. Fishbein, J. Kuebler, N. V. Vasilyev, D. J. Mooney, F. A. Pigula, and C. J. Walsh, "Soft robotic sleeve supports heart function," *Science Translational Medicine*, vol. 9, no. 373, 2017.
- [24] S. M. Babu, A. Sadeghi, A. Mondini, and B. Mazzolai, "Antagonistic pneumatic actuators with variable stiffness for soft robotic applications," in *2019 2nd IEEE International Conference on Soft Robotics (RoboSoft)*. IEEE, 2019, pp. 283–288.
- [25] Z. Saleem, "Alternatives and modifications of monopile foundation or its installation technique for noise mitigation," Delft University of Technology, Tech. Rep., 2011.
- [26] G. Gerboni, P. W. Henselmans, E. A. Arkenbout, W. R. van Furth, and P. Breedveld, "Helixflex: bioinspired maneuverable instrument for skull base surgery," *Bioinspiration & biomimetics*, vol. 10, no. 6, 2015.
- [27] J. Starke, E. Amanov, M. T. Chikhaoui, and J. Burgner-Kahrs, "On the merits of helical tendon routing in continuum robots," in *2017 IEEE/RSJ International Conference on Intelligent Robots and Systems (IROS)*. IEEE, 2017, pp. 6470–6476.
- [28] N. K. Uppalapati and G. Krishnan, "Towards pneumatic spiral grippers: Modeling and design considerations," *Soft robotics*, vol. 5, no. 6, pp. 695–709, 2018.
- [29] D. Rus and M. T. Tolley, "Design, fabrication and control of soft robots," *Nature*, vol. 521, pp. 467–475, 2015.
- [30] Y. Ansari, M. Manti, E. Falotico, M. Cianchetti, and C. Laschi, "Multiobjective optimization for stiffness and position control in a soft robot arm module," *IEEE Robotics and Automation Letters*, vol. 3, no. 1, pp. 108–115, 2017.
- [31] C. Della Santina, R. K. Katschmann, A. Biechi, and D. Rus, "Dynamic control of soft robots interacting with the environment," in *2018 IEEE International Conference on Soft Robotics (RoboSoft)*, 2018, pp. 46–53.
- [32] M. Eder, F. Hisch, and H. Hauser, "Morphological computation-based control of a modular, pneumatically driven, soft robotic arm," *Advanced Robotics*, vol. 32, no. 7, pp. 375–385, 2018.
- [33] V. Mahadevan, "Anatomy of the oesophagus," *Surgery-Oxford International Edition*, vol. 35, no. 11, pp. 603–607, 2017.
- [34] P. Boonvisut and M. C. Çavuşoğlu, "Estimation of soft tissue mechanical parameters from robotic manipulation data," *IEEE/ASME Transactions on Mechatronics*, vol. 18, no. 5, pp. 1602–1611, 2012.
- [35] Y. Sun, Y. S. Song, and J. Paik, "Characterization of silicone rubber based soft pneumatic actuators," in *2013 IEEE/RSJ International Conference on Intelligent Robots and Systems (IROS)*. Ieee, 2013, pp. 4446–4453.
- [36] T. Ranzani, G. Gerboni, M. Cianchetti, and A. Menciassi, "A bio-inspired soft manipulator for minimally invasive surgery," *Bioinspiration & biomimetics*, vol. 10, no. 3, 2015.
- [37] L. H. Blumenschein, N. S. Usevitch, B. H. Do, E. W. Hawkes, and A. M. Okamura, "Helical actuation on a soft inflated robot body," in *2018 IEEE International Conference on Soft Robotics (RoboSoft)*, 2018, pp. 245–252.